

2017-11

# Coupling cross-shore and longshore sediment transport to model storm response along a mixed sand-gravel coast under varying wave directions

Bergillos, RJ

<http://hdl.handle.net/10026.1/10217>

---

10.1016/j.coastaleng.2017.09.009

Coastal Engineering

Elsevier

---

*All content in PEARL is protected by copyright law. Author manuscripts are made available in accordance with publisher policies. Please cite only the published version using the details provided on the item record or document. In the absence of an open licence (e.g. Creative Commons), permissions for further reuse of content should be sought from the publisher or author.*

# Coupling cross-shore and longshore sediment transport to model storm response along a mixed sand-gravel coast under varying wave directions

Rafael J. Bergillos<sup>a,\*</sup>, Gerd Masselink<sup>b</sup>, Miguel Ortega-Sánchez<sup>a</sup>

<sup>a</sup>*Andalusian Institute for Earth System Research, University of Granada, Avda. del  
Mediterráneo, s/n, 18006, Granada, Spain*

<sup>b</sup>*School of Marine Science and Engineering, Plymouth University, PL4 8AA, Drake Circus,  
Plymouth, UK*

---

## Abstract

This paper investigates the profile response of a mixed sand-gravel deltaic beach (Playa Granada, southern Spain) forced by storm waves from varying directions. Beach morphology was monitored over a 36-day period with variable wave conditions, and profile response was compared to model predictions using the XBeach-G model and a longshore sediment transport (LST) formulation. XBeach-G was applied over 2-day periods of low energy, south-westerly (SW) storm and south-easterly (SE) storm conditions, and was coupled to LST using a parametric approach which distributes the LST across the swash, surf and nearshore zones. A calibrated wave propagation model (Delft3D) was used to obtain the inshore conditions required to drive the XBeach-G model and the LST formulation. The storm response is clearly influenced by the free-board (difference between the height of the berm and the total run-up) and is also strongly dependent on storm-wave direction, with the SW storm eroding the surveyed area, while the SE storm induced beach accretion. Model results indicate that XBeach-G on its own is capable of adequately reproducing the response of the beach under SW storm conditions ( $BSS > 0.95$ ), but not under SE

---

\*Corresponding author.  
E-mail address: rbergllos@ugr.es (R.J. Bergilos)

storms due to the higher LST gradients at the study location. The combination of XBeach-G and LST fits the measured profiles reasonably well under both SW ( $BSS > 0.96$ ) and SE ( $BSS > 0.88$ ) storms, inspiring confidence in the coupled model to predict the storm response under varying wave conditions. The combined XBeach-G/LST model was applied to the entire 6.8-km deltaic coastline to investigate the impact of an extreme SW and SE storm event, and the model results reiterate the importance of cross-shore and longshore sediment transport in driving coastal storm response at this location. The approach proposed in this work can be extended to other worldwide coasts highly influenced by both cross-shore and longshore sediment transport, such as beaches with different coastline orientations and/or forced by varying wave directions.

*Keywords:* Storm response, beach profile, wave propagation, XBeach-G, longshore sediment transport

---

<sup>1</sup> **1. Introduction**

<sup>2</sup> Gravel and mixed sand-gravel (MSG) beaches are common in previously  
<sup>3</sup> para-glaciated coastal regions and coasts with steep hinterlands, and are widespread  
<sup>4</sup> in the UK (Carter and Orford, 1984; Poate et al., 2016), Denmark (Clemmensen  
<sup>5</sup> and Nielsen, 2010; Clemmensen et al., 2016), Canada (Engels and Roberts,  
<sup>6</sup> 2005; Dashtgard et al., 2006), Mediterranean (Bramato et al., 2012; Bergillos  
<sup>7</sup> et al., 2016c) and New Zealand (Shulmeister and Kirk, 1993; Soons et al., 1997).  
<sup>8</sup> They are also found when nourishment projects use gravel to protect eroded  
<sup>9</sup> sandy beaches (López de San Román-Blanco, 2004; Moses and Williams, 2008).  
<sup>10</sup> Among these coastal settings, a distinction can be made between drift-aligned  
<sup>11</sup> systems (e.g., Shaw et al. (1990); Carter and Orford (1991)), where alongshore  
<sup>12</sup> sediment exchange plays the main role in driving shoreline dynamics, and swash-  
<sup>13</sup> aligned areas (e.g., Orford and Carter (1995); Orford et al. (1995)), which are

<sup>14</sup> dominated by cross-shore sediment transport (Forbes et al., 1995; Orford et al.,  
<sup>15</sup> 2002).

<sup>16</sup> Despite their societal importance, the research advances on gravel and MSG  
<sup>17</sup> beaches are limited compared to those on sandy beaches (Mason et al., 1997;  
<sup>18</sup> Jennings and Shulmeister, 2002; Pontee et al., 2004; Buscombe and Masselink,  
<sup>19</sup> 2006; López de San Román-Blanco et al., 2006; Horn and Walton, 2007). This  
<sup>20</sup> discrepancy is particularly evident for numerical approaches (Orford and An-  
<sup>21</sup> thony, 2011; Masselink et al., 2014), and contrasts strongly with the increasing  
<sup>22</sup> demand for reliable coastal change models to help mitigate and adapt to global  
<sup>23</sup> erosion problems (Syvitski et al., 2005; Anthony et al., 2014) and future sea-level  
<sup>24</sup> rise (Payo et al., 2016; Spencer et al., 2016). Several efforts have been made  
<sup>25</sup> over the last decade to develop a morphodynamic storm response model spe-  
<sup>26</sup> cific to gravel beaches (Pedrozo-Acuña, 2005; Pedrozo-Acuña et al., 2006, 2007;  
<sup>27</sup> Van Rijn and Sutherland, 2011; Jamal et al., 2011, 2014; Williams et al., 2012).  
<sup>28</sup> In the present paper, we use the XBeach-G model (McCall et al., 2012, 2013;  
<sup>29</sup> McCall, 2015), as it has been validated most extensively using both laboratory  
<sup>30</sup> and field data (McCall et al., 2014, 2015; Almeida et al., 2017).

<sup>31</sup> XBeach-G is a 1D process-based model specifically developed to model cross-  
<sup>32</sup> shore storm response on gravel beaches. However, in drift-aligned systems,  
<sup>33</sup> where longshore sediment transport (LST) plays a key role in controlling the  
<sup>34</sup> coastal behaviour (Orford et al., 1991; López-Ruiz et al., 2014), a cross-shore  
<sup>35</sup> profile model is clearly not sufficient to model storm response. Drift-aligned  
<sup>36</sup> systems could be coastlines with a highly variable shoreline orientation and a  
<sup>37</sup> uni-directional, but spatially-variable LST. Alternatively, they could be coast-  
<sup>38</sup> lines subjected to a bi-directional wave climate characterized by temporal varia-  
<sup>39</sup> tions in the frequency of the incoming wave directions and, as a consequence, in  
<sup>40</sup> the net littoral drift (French and Burningham, 2015; Bergillos et al., 2016a). In

41 these coastal areas, it is particularly important to consider not only the cross-  
42 shore sediment transport, but also the effects of LST (De Alegría-Arzaburu  
43 and Masselink, 2010; Masselink et al., 2016). Recent advances are available to  
44 estimate LST on sand, gravel and shingle beaches (Van Rijn, 2014); but the  
45 cross-shore distribution of LST, widely studied on sandy beaches (e.g., Berek  
46 and Dean (1982); Komar (1983); Kamphuis (1991); Bayram et al. (2001)) and  
47 relevant for modelling coastal response, has not been investigated in depth on  
48 gravel and MSG beaches (Van Wellen et al., 1998; Van Wellen et al., 2000).

49 The main objectives of this paper are to characterize and to model the storm  
50 response of an MSG beach (Playa Granada, southern Spain) under varying  
51 wave directions. Thirteen field surveys were performed and a numerical model  
52 (Delft3D) calibrated for the study site was used to relate the wave propagation  
53 patterns with the coastal dynamics. Delft3D results were also used to apply  
54 and test the XBeach-G model forced by low energy (LE) conditions, and south-  
55 westerly (SW) and south-easterly (SE) storms. In addition, XBeach-G was  
56 combined with the LST equation of Van Rijn (2014) by means of a parametric  
57 formulation to consider different cross-shore distributions of LST. Finally, the  
58 approach that best fitted the observed response was used to model extreme  
59 SE and SW storms along the entire deltaic coastline, highlighting the potential  
60 of the proposed coupled model to extend XBeach-G towards larger longshore  
61 scales.

## 62 **2. Study site**

63 Playa Granada is a 3-km long micro-tidal beach located on the southern coast  
64 of Spain that faces the Mediterranean Sea (Figure 1). The beach corresponds  
65 to the central stretch of the Guadalfeo deltaic plain (Bergillos et al., 2015c) and  
66 is bounded to the west by the Guadalfeo River mouth and to the east by *Punta*

*del Santo*, the former location of the river mouth (Figure 1). The deltaic coast is bounded to the west by Salobreña Rock and to the east by Motril Harbour.

This harbour is an artificial barrier that prevents LST (Félix et al., 2012).

The Andalusian littoral of the Mediterranean Sea is characterized by the presence of high mountainous relief angles and short fluvial streams. The Guadalete River contributes most sediment to the beach (Bergillos et al., 2016d). Its basin covers an area of 1252 km<sup>2</sup>, including the highest peaks on the Iberian Peninsula ( $\sim$  3400 m.a.s.l.), and the river is associated with one of the most high-energy drainage systems along the Spanish Mediterranean coast. These steep topographic gradients lead to a wide range of sediment sizes in the Guadalete river sediment load (Millares et al., 2014).

Consequently, the particle size distribution on the coast is particularly complex, with varying proportions of sand and gravel. Although three sediment fractions are predominant in the studied coastal area –sand (0.35 mm), fine gravel (5 mm) and coarse gravel (20 mm)– (Bergillos et al., 2015a), the morphodynamic response of the beach is dominated by the coarse gravel fraction due to the selective removal of the finer material (Bergillos et al., 2016c) and the reflective shape of the profile is similar to those found on gravel beaches (Masselink et al., 2010; Poate et al., 2013). Previous numerical works also demonstrated that the best fits to the measured profiles (Bergillos et al., 2016b) and shorelines (Bergillos et al., 2017) are obtained by assuming that the beach is made up of coarse gravel.

The river was dammed 19 km upstream from the mouth in 2004, regulating 85% of the basin run-off (Losada et al., 2011). The total capacity of the Rules' Reservoir (117 hm<sup>3</sup>) was planned to be used for the following purposes: irrigation (40%), supplies for residential developments along the coast (19%), energy generation (9%), flood control (30%) and environmental flow (2%). However,

94 as a consequence of river damming, the delta currently experiences coastline  
95 retreat and severe erosion problems (Bergillos and Ortega-Sánchez, 2017). The  
96 stretch of beach examined, which is occupied by an exclusive hotel complex,  
97 golf courses, restaurants and summer homes (Félix et al., 2012), has been par-  
98 ticularly affected and has been subjected to higher levels of coastline retreat in  
99 recent years than both western and eastern stretches, known as Salobreña and  
100 Poniente Beach, respectively (Bergillos et al., 2015b).

101 Climatic patterns at the study site exhibit a significant contrast between  
102 summer and winter. The region is subjected to the passage of extra-tropical  
103 Atlantic cyclones and Mediterranean storms with average wind speeds of 18–  
104 22 m/s (Ortega-Sánchez et al., 2017) which generate wind waves under fetch-  
105 limited conditions (approximately 200 to 300 km). The storm wave climate  
106 is bimodal with prevailing W-SW (extra-tropical cyclones) and E-SE (Mediter-  
107 ranean storms) wave directions. The 90%, 99% and 99.9% exceedance significant  
108 wave heights in deep water are 1.2 m, 2.1 m and 3.1 m, respectively. The astro-  
109 nomical tidal range is  $\sim$  0.6 m, whereas typical storm surge levels can exceed  
110 0.5 m (Bergillos et al., 2016c).

### 111 3. Methodology

#### 112 3.1. Maritime data and total run-up

113 A 36-day time series of 864 sea states (hourly hindcasted data for the study  
114 period), corresponding to SIMAR point number 2041080 (Figure 1) and pro-  
115 vided by *Puertos del Estado*, was used to study the evolution of the following  
116 deep-water wave and wind variables: significant wave height ( $H_0$ ), spectral peak  
117 period ( $T_p$ ), wave direction ( $\theta_0$ ), wind velocity ( $V_w$ ) and wind direction ( $\theta_w$ ).  
118 They were also used as boundary conditions to apply the wave propagation  
119 model.

In addition, the total run-up ( $\eta$ ) was estimated as the sum of astronomical tide (measured by a gauge located in the Motril Harbour), wind set-up ( $\Delta\eta_{\text{wind}}$ ), barometric set-up ( $\Delta\eta_{\text{bar}}$ ) and wave run-up ( $\Delta\eta_{\text{wave}}$ ). The wind set-up was calculated as  $\Delta\eta_{\text{wind}} = \tau_{\text{wind}}/(\rho gh_0) \Delta x$  (Bowden, 1983), where  $g$  is the acceleration of gravity,  $\rho = 1025 \text{ kg/m}^3$  is the density of salt water,  $\Delta x$  is the wave fetch from the centre of the low-pressure system to the coast (estimated through isobar maps), the depth of the wave base level is represented by  $h_0 = L_0/4$ , where  $L_0$  is the wavelength in deep water, and the tangential wind stress is obtained from  $\tau_{\text{wind}} = \rho_a U_*^2$ , where  $\rho_a$  is the air density and  $U_*$  is the friction velocity. The barometric set-up was calculated as  $\Delta\eta_{\text{bar}} = \Delta P_a/(\rho g)$  (Dean and Dalrymple, 2002), where  $\Delta P_a$  represents the atmospheric pressure variation relative to the long-term average pressure at Motril Harbour. The wave run-up was estimated as  $\Delta\eta_{\text{wave}} = 0.36 g^{0.5} H_{8,0}^{0.5} T_p \tan \beta$  (Nielsen and Hanslow, 1991), where  $\tan \beta$  is the intertidal slope and  $H_{8,0}$  is the modelled wave height at 8 m water depth de-shoaled to deep water using linear theory and assuming parallel bottom contours. Bergillos et al. (2016c) obtained high correlation (differences less than 9%) between measured and estimated total run-up values with these formulations.

### 3.2. Field measurements

Thirteen topographic surveys were performed during the 36-day study period (Table 1) to measure the morphology of the beach profile in the central area of the stretch river mouth - *Punta del Santo* (Figure 1). This coastal section is considered representative of the beach behaviour of that section of the coastline (Bergillos et al., 2016c). Each survey was performed under low tide conditions and the observations were referenced to the mean low water spring (MLWS) level.

Topographic measurements were carried out using a highly accurate DGPS

| Survey | S1   | S2   | S3   | S4   | S5   | S6   | S7   | S8   | S9  | S10 | S11 | S12  | S13  |
|--------|------|------|------|------|------|------|------|------|-----|-----|-----|------|------|
| Date   | 15/1 | 16/1 | 18/1 | 20/1 | 22/1 | 23/1 | 27/1 | 30/1 | 2/2 | 6/2 | 9/2 | 13/2 | 20/2 |

Table 1: Timeline of the profile surveys carried out during the study period.

147 (Javad Maxor) with less than 0.02 m of instrument error. Eleven equally-spaced  
148 (10 m) shore-normal profiles were measured (Figure 1) and combined to ob-  
149 tain an alongshore-averaged profile representative of the surveyed area. This  
150 alongshore-averaged beach profile was used to address the evolution of the beach  
151 under varying wave conditions, as well as for comparison with model predictions.

152 A high-resolution multibeam bathymetric survey was performed at the be-  
153 ginning of the study period covering the entire deltaic region. Data were ac-  
154 quired using Differential Global Positioning System (DGPS) navigation in refer-  
155 ence to the WGS-84 ellipsoid. Accurate navigation and real-time pitch, roll and  
156 heave were corrected. A topographic survey along the entire deltaic beach was  
157 carried out simultaneously to complement the multibeam bathymetry. These  
158 morphological data were used as the bottom boundary conditions for the wave  
159 propagation model. To calibrate this model, wave data were continuously col-  
160 lected from December 20th, 2014 to January 30th, 2015 by means of two ADCPs  
161 (Figure 1).

162 *3.3. Numerical modelling*

163 *3.3.1. Wave propagation model: Delft3D*

164 SIMAR point data for the entire study period (Section 3.1) were propagated  
165 from deep-water areas to the nearshore using the WAVE module of the Delft3D  
166 model (Lesser et al., 2004; Lesser, 2009), which is based on the SWAN model  
167 (Holthuijsen et al., 1993). These results were used to address inshore wave  
168 conditions and to provide the boundary conditions for the XBeach-G model  
169 and the LST formulation.

170 The model domain consisted of two different grids, shown in Figure 1. The

171 first is a coarse curvilinear 82x82-cell grid covering the entire deltaic region, with  
172 cell sizes that decrease with depth from 170x65 to 80x80 m. The second is a  
173 nested grid covering the beach area with 244 and 82 cells in the alongshore and  
174 cross-shore directions, respectively, and with cell sizes of approximately 25x15 m.  
175 This model was calibrated for the study site by Bergillos et al. (2016a) through  
176 comparison with field data, obtaining coefficients of determination equal to 0.86  
177 and 0.89 for the ADCPs A1 and A2 (Figure 1), respectively.

178 *3.3.2. Morphodynamic model of the beach profile: XBeach-G*

179 The 1D process-based model XBeach-G is an extension of the XBeach model  
180 that incorporates: (1) a non-hydrostatic pressure correction term that allows  
181 solving waves explicitly in model; (2) a groundwater model that allows infiltration  
182 and exfiltration; and (3) the computation of bed load transport, including  
183 the effects of groundwater ventilation and flow acceleration forces, for estimating  
184 bed level changes (McCall et al., 2014, 2015; Masselink et al., 2014).

185 Bergillos et al. (2016b) has shown that the model is capable of reproducing  
186 the morphodynamic response of the beach at the study site under SW storms for  
187 a grain size of 20 mm; however, it has not been tested under SE waves. For this  
188 reason, XBeach-G was applied to model the profile response of the surveyed area  
189 during three 2-day wave windows, depicted in Figure 2, which are representative  
190 of LE, SW storm and SE storm conditions. Values of sediment friction factor  
191 and Nielsen's boundary layer phase lag used for the simulations were 0.03 and  
192 20°, respectively, which were found to be optimum during the calibration of the  
193 model (Bergillos et al., 2016b). These values are slightly different to those found  
194 on pure gravel beaches (0.01 and 25°, respectively) by Masselink et al. (2014)  
195 and McCall (2015).

196 Measured topographic data during surveys 6, 7 and 11 were used as initial  
197 condition of the upper profile (beach profile above the MLWS level) for the

198 LE, SW and SE cases, respectively. Measured bathymetric data were used as  
 199 initial lower profile (beach profile below the MLWS level) for the LE and SW  
 200 cases since morphological changes between surveys 1 and 7 were comparatively  
 201 insignificant, whereas the final lower profile for the SW case was used as initial  
 202 condition for the SE storm. The input wave boundary conditions were obtained  
 203 from the Delft3D-WAVE model at a depth of 10 m. This water depth offshore  
 204 boundary fulfils all requirements detailed in the manual of the XBeach-G model  
 205 (Deltares, 2014), and is deeper than the maximum closure depth in the study  
 206 site ( $\sim 9$  m according to Bergillos et al. (2016d) and Bergillos et al. (2017)).  
 207 The infrastructure associated with the hotel complex located landward of the  
 208 surveyed area (Figure 1) was included in the cross-shore profile as a non-erodible  
 209 object.

### 210 *3.3.3. Longshore sediment transport: formulation and cross-shore distribution*

211 To model LST and the ensuing changes in the upper profile, the LST ex-  
 212 pression proposed by Van Rijn (2014), which was deduced for sand, gravel and  
 213 shingle beaches, was applied:

$$Q_m = 0.00018 K_{vr} \rho_s g^{0.5} (\tan \beta)^{0.4} D_{50}^{-0.6} H_b^{3.1} \sin(2\theta_b) \quad (1)$$

214 where  $Q_m$  is the LST rate (dry mass, in kg/s),  $K_{vr}$  is a wave correction factor  
 215 that accounts for the effect of the wave period on the LST rate,  $\rho_s = 2650$  kg/m<sup>3</sup>  
 216 is the sediment density,  $\tan \beta$  is the beach slope,  $D_{50}$  is the sediment size,  $H_b$   
 217 is the significant wave height at breaking and  $\theta_b$  is the wave angle from shore-  
 218 normal at breaking.

219 The expression was applied considering alongshore variations in the shore-  
 220 line, wave variables and beach slope. Surf zone parameters were calculated based  
 221 on the results of the wave propagation model, obtaining breaking conditions for

222 69 (shore-normal) beach profiles equally distributed (1 every 100 m) along the  
 223 coastline between Salobreña Rock and Motril Harbour. The application of this  
 224 formulation for the coarse gravel fraction ( $D_{50} = 20$  mm) was found to provide  
 225 the best fit to measured morphological changes of the shoreline in the study site  
 226 (Bergillos et al., 2017). LST gradients were obtained as the ratio between the  
 227 differences in LST rates among consecutive beach profiles (boundaries) and the  
 228 distance between them (100 m).

229 For the cross-shore distribution of the modelled LST volume gradients per  
 230 meter of shoreline, the following equation was proposed:

$$q = a \frac{x}{x_b} \exp\left(-k \frac{x}{x_b}\right) \quad (2)$$

231 where  $q$  (in m) is the cross-shore distribution of the LST volume gradient ( $V$ ,  
 232 in  $\text{m}^3/\text{m}$ ),  $x$  is the length across the beach profile ( $x = 0$  represents the position  
 233 of the total run-up),  $x_b = s_R + s_b$ , where  $s_R$  is the length (across the profile)  
 234 between the total run-up limit and the shoreline, and  $s_b$  is the length (across the  
 235 profile) between the shoreline and the breaking line. The constant  $k$  determines  
 236 where the peak of the cross-shore distribution is located ( $k x/x_b = 1$ ), whereas  
 237 the parameter  $a$  (in m) is obtained numerically as a function of  $V$  and  $x_b$  through  
 238 the following equation:

$$V = \frac{\partial Q}{\partial l} \Delta t = \int_0^{x_b} q(x) dx = \int_0^{x_b} a \frac{x}{x_b} \exp\left(-k \frac{x}{x_b}\right) dx \quad (3)$$

239 Through modification of  $k$ , this approach can reproduce relatively symmet-  
 240 rical cross-shore distributions of LST reported for sandy beaches (e.g, Bayram  
 241 et al. (2001)), as well as the asymmetrical distributions on MSG and gravel  
 242 beaches, whose peaks are expected to be located landward of the peaks on  
 243 sandy beaches due to the importance of swash processes in gravel environments

244 (Buscombe and Masselink, 2006). In this work, the profiles resulting from the  
245 three values of  $k$  were tested, compared and optimised against the observed  
246 profile changes ( $k_1 = 2$ ,  $k_2 = 5$ ,  $k_3 = 10$ ).

247 *3.3.4. Coupling XBeach-G and longshore sediment transport*

248 The three 2-day windows of varying wave conditions selected to apply the  
249 XBeach-G model (indicated in Figure 2) were also simulated through the com-  
250 bination of XBeach-G and LST. For that, the shape of the final beach profile  
251 modelled with XBeach-G was modified after each sea-state considering the LST  
252 volume gradients and the three cross-shore distributions of LST detailed in Sec-  
253 tion 3.3.3.

254 The goodness of fit for each approach was evaluated through the root-mean-  
255 square error (RMSE, in m), the relative bias normalised by the absolute mean of  
256 the observations (bias), the correlation coefficient ( $\rho$ ) and the Brier Skill Score  
257 (BSS). All statistics were computed using data interpolated to a regularly-spaced  
258 grid and including only points where the measured or modelled bed level changes  
259 were greater than the maximum between the estimated instrument error and  
260  $3D_{50}$ , according to McCall et al. (2015). Following the criteria proposed by  
261 Van Rijn et al. (2003), the fits were qualified from *bad* to *excellent* based on the  
262 BSS values.

263 Finally, the impact of extreme SW and SE storms ( $H_{99.9\%}$ ) was modelled  
264 using both XBeach-G and the coupled model for the entire 6.8-km deltaic coast-  
265 line to further determine the importance of cross-shore and longshore sediment  
266 transport in driving storm response under varying wave directions. The mod-  
267 elled wave variables were  $H_0 = 3.1$  m,  $T_p = 8.4$  s (the most frequent period  
268 under storm conditions),  $\theta_{0,SW} = 238^\circ$  and  $\theta_{0,SE} = 107^\circ$  (the most frequent  
269 directions under SW and SE storms, respectively). These sea states, summa-  
270 rized in Table 2, were simulated considering a storm surge ( $\eta_{ss}$ ) of 0.5 m for two

<sup>271</sup> different durations: 6 hours around high tide and 12 hours representing a full  
<sup>272</sup> tidal cycle.

|                           | SW storm | SE storm |
|---------------------------|----------|----------|
| $H_0$ (m)                 | 3.1      | 3.1      |
| $T_p$ (s)                 | 8.4      | 8.4      |
| $\theta_0$ ( $^{\circ}$ ) | 238      | 107      |
| $\eta_{ss}$               | 0.5      | 0.5      |

Table 2: Sea-states modelled with XBeach-G and XBeach-G/LST to study storm response under varying wave directions along the entire deltaic coastline.

## <sup>273</sup> 4. Results

### <sup>274</sup> 4.1. Wave, wind and water level conditions

<sup>275</sup> The deep-water significant wave height and the spectral peak period were  
<sup>276</sup> lower than 1 m and 6 s during the 56.3% and 62% of the study period, re-  
<sup>277</sup> spectively (Figure 2a-b). These values are significantly lower than average per-  
<sup>278</sup> centages from January 1958 till the end of the study period (84.6% and 83.8%,  
<sup>279</sup> respectively, based on the SIMAR 2041080 data), indicating that the beach was  
<sup>280</sup> forced by relatively high energy waves during this 36-day period. The predom-  
<sup>281</sup> inant deep-water wave directions were  $180^{\circ} < \theta_0 < 270^{\circ}$  (SW sector, 50.9%  
<sup>282</sup> of the time) and  $90^{\circ} < \theta_0 < 180^{\circ}$  (SE sector, 36% of the time). This period  
<sup>283</sup> was, thus, more westerly-dominated than the average (41.6% and 55.7%, re-  
<sup>284</sup> spectively), in agreement with the trend in wave direction over last six years  
<sup>285</sup> (Bergillos et al., 2016a). The average wind velocity was 7.4 m/s, with prevailing  
<sup>286</sup> values less than 10 m/s (73.3% of the time) and incoming directions from the  
<sup>287</sup> W-SW and E-SE (Figure 2d).

<sup>288</sup> Two extreme storms ( $H_0 > H_{99.9\%}$ ) occurred with maximum  $H_0$  of 4.9 m and  
<sup>289</sup> 3.2 m, and maximum  $T_p$  equal to 9.2 s and 8.4 s, respectively. The first storm,  
<sup>290</sup> which occurred between surveys 7 and 9 (S7-S9), was associated with westerly  
<sup>291</sup> waves ( $\theta_0 \in [235^{\circ}, 239^{\circ}]$ ); whereas the second storm, during period S11-S12, was  
<sup>292</sup> forced by easterly waves ( $\theta_0 \in [104^{\circ}, 117^{\circ}]$ ). The maximum  $V_w$  during storms

1 and 2 were 19.9 m/s and 16.5 m/s with  $\theta_w$  from the W-SW (extra-tropical  
Atlantic cyclone) and the E-SE (Mediterranean storm), respectively. The SW  
storm was the second most severe since 1958. The maximum total run-up (sum  
of the astronomical tide, storm surge and wave run-up) during this storm was  
2.6 m (Figure 2e), generating overwash along the entire beach profile (Section  
4.3).

#### 4.2. Wave propagation patterns in the nearshore zone

Figure 3 depicts the spatial distribution of the time-averaged energy flux  
(in W/m) between surveys 1-7, 7-10 and 10-13 according to Delft3D-WAVE  
modelling. Nearshore wave energy levels were comparatively insignificant during  
S1-S7 (Figure 3a), when the average wave height ( $H_0 = 0.62$  m), mean period  
( $T_z = 2.95$  s) and peak period ( $T_p = 4.19$  s) were the lowest, and the percentages  
of SW-SE waves were the most balanced (46.9%-30.5%). Between S7 and S10,  
the highest values of nearshore wave energy were concentrated in the studied  
section of coastline due to the prevailing SW waves during this period (Figure  
2c).

Nearshore wave energy levels between S10 and S13 were significantly lower  
than those over the period S7-S10 (Figure 3b-c). Considering that the average  
values of mean and peak wave periods were similar ( $T_z = 4.13$  s and  $T_p = 6.01$   
s during S7-S10 vs  $T_z = 4.15$  s and  $T_p = 6.26$  during S10-S13), the lower  
energy levels over S10-S13 are attributable to both the less average wave height  
( $H_0 = 1.54$  m vs  $H_0 = 1.34$  m) and the more balanced percentages of SW-SE  
waves (75.8%-4.6% vs 36.7%-63.1%). The dominance of SE waves during S10-  
S13 generated higher energy levels along the section *Punta del Santo - Motril*  
Harbour compared to those in Playa Granada (Figure 3c). This highlights the  
importance of the incoming wave directions in the nearshore wave propagation  
patterns, with direct implications in the profile response.

320 *4.3. Observed morphological response of the upper profile*

321 Three different profile responses were observed during the study period (Figure 4). The morphological changes were relatively insignificant between S1 and S7 due to the lower total run-up and energy level over this period (Figures 2e and 3a), but the profile strongly eroded during S7-S9 induced by the extreme SW storm. The profile could not be completely measured during S8 since it coincided with the beginning of the overwash (Figure 5a); therefore, the morphology of this profile at elevations below 1.5 m should be taken with caution (Figure 4b). Beach recovery occurred between S10 and S13 influenced by the medium energy content during this period (Figures 3c and 4c). This is in agreement with observations of Bramato et al. (2012) on a nearby MSG beach, who found that a minimum wave energy is required not only to erode the beach, but also to recover it. It is suggested, and demonstrated in Section 4.5, that the SE storm between S11 and S12 contributed to this recovery due to LST.

334 Figure 6 depicts the maximum total run-up, the minimum free-board (difference between the height of the berm and the maximum total run-up) and the volumetric changes above the MLWS level (in  $\text{m}^3$  per unit m of shoreline, or  $\text{m}^2$ ) between surveys. It is observed how between S1 and S7, dominated by swash regime, accretion rates were lower than  $0.36 \text{ m}^2/\text{day}$ ; whereas between S7 and S9, when overwash occurred, the average erosion rate was  $2.56 \text{ m}^2/\text{day}$ . Beach recovery up to  $1.1 \text{ m}^2/\text{day}$  took place between S9 and S13, with positive values of the free-board over this whole period. The destruction of the berms between S7 and S9 and the subsequent generation of new berm deposits are also observed in the lower panel of Figure 6, which shows the cross-shore distribution of the bed level changes between surveys. These patterns confirm the importance of the overwash process (Matias et al., 2014) and the total run-up (Bergillos et al., 2016c) dictating beach response.

<sup>347</sup> 4.4. Modelling profile response with XBeach-G

<sup>348</sup> Figure 7 shows the initial, final measured and final modelled profiles with  
<sup>349</sup> XBeach-G, along with the differences in the cross-shore distance measured  
<sup>350</sup> ( $\Delta X_{\text{Meas}}$ ) and predicted ( $\Delta X_{\text{Mod}}$ ) for the three temporal windows indicated in  
<sup>351</sup> Figure 2. As expected, the XBeach-G model does not reproduce the relatively  
<sup>352</sup> small ( $\Delta X_{\text{Meas}} < 0.5$  m) accretional changes observed under LE conditions;  
<sup>353</sup> however, the fit between modelled and measured bed level variations forced by  
<sup>354</sup> the SW storm is *excellent* ( $BSS = 0.96$ ), with  $RMSE < 0.14$  m and bias < 0.13  
<sup>355</sup> (Table 3). This indicates that the model is capable of reproducing the response  
<sup>356</sup> of the studied coastline section under SW storm conditions, which is in agree-  
<sup>357</sup> ment with previous results of the model for two less energetic SW storms in  
<sup>358</sup> December 2013 and March 2014 (Bergillos et al., 2016b).

<sup>359</sup> The comparison of pre- and post-storm measured profiles under SE waves  
<sup>360</sup> reveals that accretion took place across the upper profile. This deposition was  
<sup>361</sup> mainly concentrated at an elevation of 1.2–1.3 m, coinciding with the total run-  
<sup>362</sup> up during this window (Figure 2e) and contrasting with the erosion predicted  
<sup>363</sup> by the model at this location (Figure 7c). This behaviour is influenced by  
<sup>364</sup> the higher LST gradients for SE storms with respect to those for SW conditions  
<sup>365</sup> (Section 4.5), and highlights the need to combine the XBeach-G results with LST  
<sup>366</sup> gradients to provide more confident predictions of the morphological response  
<sup>367</sup> under SE storm conditions.

|            | Low energy conditions |        |        |       | South-westerly storm |       |        |       | South-easterly storm |        |        |       |
|------------|-----------------------|--------|--------|-------|----------------------|-------|--------|-------|----------------------|--------|--------|-------|
|            | RMSE                  | bias   | $\rho$ | BSS   | RMSE                 | bias  | $\rho$ | BSS   | RMSE                 | bias   | $\rho$ | BSS   |
| XBeach-G   | 0.02                  | -0.73  | 0.117  | 0.007 | 0.134                | 0.125 | 0.966  | 0.956 | 0.175                | -1.122 | 0.564  | 0.137 |
| LST (k=2)  | 0.015                 | -0.076 | 0.519  | 0.453 | 0.103                | 0.091 | 0.967  | 0.962 | 0.082                | -0.503 | 0.91   | 0.768 |
| LST (k=5)  | 0.014                 | -0.068 | 0.523  | 0.457 | 0.09                 | 0.072 | 0.966  | 0.964 | 0.057                | -0.269 | 0.938  | 0.887 |
| LST (k=10) | 0.015                 | 0.074  | 0.521  | 0.455 | 0.092                | -0.11 | 0.961  | 0.963 | 0.099                | 0.516  | 0.929  | 0.662 |

Table 3: Root-mean-square error (RMSE, in m), relative bias (bias), correlation coefficient ( $\rho$ ) and Brier Skill Score (BSS) of the modelled changes relative to the measurements of the upper profile.

368 4.5. Modelling profile response with XBeach-G and longshore sediment transport

369 To couple XBeach-G and longshore processes, LST rates along the entire  
370 deltaic coastline were computed for the three 2-day windows on the basis of  
371 the formulation of Van Rijn (2014), detailed in Section 3.3.3. The results in-  
372 dicate that the time-averaged LST rates during the SW storm were greater in  
373 the section *Punta del Santo* - Motril Harbour (up to  $0.038 \text{ m}^3/\text{s}$ ) than in the  
374 studied section (up to  $0.02 \text{ m}^3/\text{s}$ ). However, the opposite occurred over the SE  
375 storm, except in the vicinity of Motril Harbour, where the shoreline alignment  
376 is NW-SE, inducing higher breaking angles from shore-normal (Figure 8). The  
377 maximum and time-averaged LST rates (in absolute value) along the section  
378 Guadalfeo River mouth - *Punta del Santo* during the SE storm were up to  
379  $0.025 \text{ m}^3/\text{s}$  ( $90 \text{ m}^3/\text{h}$ ) and  $0.013 \text{ m}^3/\text{s}$  ( $46.8 \text{ m}^3/\text{h}$ ), respectively. These values  
380 were similar to those under the SW storm ( $0.022 \text{ m}^3/\text{s}$  and  $0.02 \text{ m}^3/\text{s}$ , respec-  
381 tively), which was a significantly more energetic window ( $H_{\max,\text{SW}} = 4.9 \text{ m}$  and  
382  $H_{\text{mean,SW}} = 3.2 \text{ m}$  vs  $H_{\max,\text{SE}} = 3.2 \text{ m}$  and  $H_{\text{mean,SE}} = 2.1 \text{ m}$ ), revealing the  
383 importance of LST in this coastal section forced by SE conditions. The average  
384 LST rates over the LE window were two orders of magnitude lower than those  
385 obtained for both storms (Figure 8).

386 Figure 9 details the LST rates during the entire study period for the surveyed  
387 area, whose boundaries are indicated in Figures 1 and 8. It is observed that  
388 the difference in breaking angles and LST rates between the two boundaries  
389 was greater under SE wave conditions, inducing higher gradients in the LST  
390 rates and volumes. In addition, the breaking depths and cross-shore distances  
391 were significantly lower over the SE storm window than those during the SW  
392 window, i.e., LST was concentrated in a smaller width across the nearshore  
393 zone, resulting in higher bed level changes across the upper beach profile for the  
394 SE storm. To model this cross-shore distribution of LST volume, three different

395 options were tested based on the parametric approach reported in Section 3.3.3.

396 The cross-shore distributions for each sea state of the three modelled windows  
397 are shown in Figure 10. The LST distribution for  $k = 2$  is the most  
398 uniform with the maximum located in the middle between the total run-up  
399 limit and the breaking line (at  $x/x_b = 0.5$ ). This distribution is similar to that  
400 previously observed on sandy beaches (Berek and Dean, 1982; Bayram et al.,  
401 2001). The LST distribution for  $k = 10$  is the most asymmetrical with the  
402 maximum located at  $x/x_b = 0.1$ , concentrating most of the LST in the inner  
403 nearshore region (Figure 10a3-d3). This behaviour is considered more typical  
404 of gravel beaches, where the surf zone does not exist and most of the sediment  
405 transport occurs in the swash zone (Buscombe and Masselink, 2006). The LST  
406 distribution for  $k = 5$  is intermediate between the previous two, with the maxi-  
407 mum located at  $x/x_b = 0.2$ , which is suggested to be expected for MSG beaches.  
408 These three cross-shore distributions were used to combine XBeach-G and LST,  
409 updating the morphology of the beach profile after each sea state by means of  
410 the computed total run-up locations, breaking lengths across the profile and  
411 LST volume gradients (Figure 9).

412 The results of the coupling for the three simulated windows and the three  
413 tested cross-shore distributions are shown in Figure 11. The goodness-of-fit  
414 parameters obtained for the different model approaches are summarized in Table  
415 3. The best model performance (lower RMSE-bias and higher  $\rho$ -BSS) is obtained  
416 for the combination of XBeach-G and LST considering the intermediate cross-  
417 shore distribution of LST ( $k = 5$ , Figure 10a2-d2), with the only exception of  
418 the slightly higher  $\rho$  with  $k = 2$  for the SW storm (Table 3). The intermediate  
419 approach improves the XBeach-G results for LE easterly conditions, although  
420 the fit for this case is only *fair* ( $BSS = 0.46$ ). However, the obtained fits for both  
421 SW and SE storms are *excellent* ( $BSS = 0.96$  and  $BSS = 0.89$ , respectively),

422 inspiring confidence in the proposed approach to model the storm response  
423 under varying wave conditions. The improvements with respect to the XBeach-  
424 G results are primarily relevant under SE storms ( $|\Delta\text{RMSE}| > 0.11 \text{ m}$ ,  $|\Delta\text{bias}| >$   
425  $\Delta\rho > 0.37$  and  $\Delta\text{BSS} > 0.7$ ). These results reveal the importance of LST  
426 on the coastal response of the surveyed area under SE wave conditions.

427 *4.6. Storm response along the coastline under varying wave directions*

428 Figure 12 depicts the volumetric changes of the upper profile along the entire  
429 6.8-km deltaic coastline modelled with XBeach-G and through the combination  
430 of XBeach-G and LST for  $k = 5$ . It is observed how XBeach-G predicts beach  
431 erosion along most of the coastline, with only some relatively low depositional  
432 changes in the stretch Salobreña Rock - *Punta del Santo* (western section) and  
433 *Punta del Santo* - Motril Harbour (eastern section) for SE and SW storms,  
434 respectively. As expected, volumetric changes on the basis of the XBeach-G  
435 results are significantly higher along the western (eastern) section under SW  
436 (SE) storms (Figure 12b1-b2).

437 Results with the coupled model for SW storm conditions show more erosion  
438 than those obtained with XBeach-G along most of the western section, and also  
439 show accretion rather than erosion along most of the eastern section (Figure  
440 12b1-c1). Under SE storms, the combined approach reverts XBeach-G results  
441 along the section Guadalefo River mouth - *Punta del Santo* (Figure 12b2-c2),  
442 predicting depositional rather than erosional changes, and in agreement with the  
443 observations reported in Section 4.3. Results along the eastern section reveal  
444 larger erosion than XBeach-G predictions in the vicinity of *Punta del Santo* and  
445 accretion instead of erosion near Motril Harbour, influenced by the LST patterns  
446 at these locations under SE storms. The variations between both models for  
447 such conditions are significantly lower in the stretch Salobreña Rock - Guadalefo  
448 River mouth due to the less LST gradients along this section under SE waves

<sup>449</sup> (Figure 8).

<sup>450</sup> The comparison between the two simulated periods indicates that most of  
<sup>451</sup> the morphological changes are induced by cross-shore and longshore sediment  
<sup>452</sup> transport during high tide. During low tide conditions, beach recovery takes  
<sup>453</sup> place at some locations of the western (eastern) section under SW (SE) storms  
<sup>454</sup> (Figure 12), highlighting the importance of the total run-up and overwash pro-  
<sup>455</sup> cess dictating beach response. The results of this section show the potential  
<sup>456</sup> of the coupled approach proposed in this work to provide more confident pre-  
<sup>457</sup> dictions of the storm response on coasts dominated by both cross-shore and  
<sup>458</sup> longshore sediment transport.

<sup>459</sup> **5. Conclusions**

<sup>460</sup> Although gravel and MSG coasts have received increasing attention during  
<sup>461</sup> recent years, relatively few numerical models have been applied to and compared  
<sup>462</sup> with field data for these coastal settings. This paper studies and models the  
<sup>463</sup> storm response of Playa Granada (southern Spain) under varying wave direc-  
<sup>464</sup> tions by means of field measurements, the application of the XBeach-G model  
<sup>465</sup> and the proposal of a parametric approach to couple XBeach-G and LST. Based  
<sup>466</sup> on the observations and results, the following conclusions were drawn:

- <sup>467</sup> 1. The morphological storm response is clearly related to the difference be-  
<sup>468</sup> tween the height of the berm and the total run-up (i.e., the free-board).  
<sup>469</sup> Wave propagation patterns are influenced by the incoming wave direc-  
<sup>470</sup> tions, generating varying values of total run-up and resulting in different  
<sup>471</sup> beach responses, with the SW and SE storms eroding and building up the  
<sup>472</sup> surveyed area, respectively.
- <sup>473</sup> 2. The XBeach-G model is capable of reproducing the storm response of  
<sup>474</sup> the beach under SW waves, with  $BSS > 0.95$  and a relative bias  $< 0.13$ .

475 However, the accretionary response of the upper profile under SE storms  
476 contrasts with the erosion predicted by the model ( $BSS < 0.14$  and  $|bias| >$   
477  $1.12$ ). This is influenced by the higher LST gradients under SE storms at  
478 the study location compared to those under SW conditions, revealing the  
479 necessity to combine XBeach-G with LST.

480 3. The coupling of XBeach-G and the LST equation of Van Rijn (2014),  
481 through consideration of different cross-shore distributions of LST, im-  
482 proved the model predictions, especially under SE storm conditions. The  
483 best fits ( $BSS > 0.96$  and  $BSS > 0.88$  for the SW and SE storms, re-  
484 spectively) were obtained with a distribution where the peak of the LST  
485 volume is located at a distance from the total run-up limit equal to 20% of  
486 the length across the profile between this limit and the breaking line, pro-  
487 viding insights into the cross-shore distribution of LST on MSG beaches.

488 4. The approach that best fitted the beach response was applied to model  
489 extreme SW and SE storms along a 6.8-km section of deltaic coastline.  
490 Erosional changes were obtained along most of the western section for  
491 the SW storm, and in the eastern section and to the west of the river  
492 mouth for the SE storm. Erosion occurred in particular under high tide  
493 conditions. In contrast, the coupled model predicted accretion along most  
494 of the eastern section and in the stretch river mouth - *Punta del Santo*  
495 under SW and SE storms, respectively. These depositional responses were  
496 not predicted by the XBeach-G model on its own. Thus, the approach  
497 proposed in this paper represents an extension of XBeach-G to make it  
498 more suitable for gravel and MSG coasts highly influenced by both cross-  
499 shore and longshore sediment transport.

500      **Acknowledgements**

501      This research was supported by the project CTM2012-32439 (Secretaría de  
502      Estado de I+D+i, Spain) and the research group TEP-209 (Junta de Andalucía).  
503      Rafael J. Bergillos was funded by the Ministry of Economy and Competitive-  
504      ness (Spain) through Research Contract BES-2013-062617 and Mobility Grants  
505      EEBB-I-15-10002 and EEBB-I-16-11009. Gerd Masselink was funded by EP-  
506      SRC grant EP/H040056/1 and NERC grant NE/N015525/1. We would like to  
507      thank Robert T. McCall and Miguel A. Losada for their helpful advice. We also  
508      acknowledge two anonymous reviewers for their improvements to this paper.

509      **References**

- 510      Almeida, L.P., Masselink, G., McCall, R., Russell, P., 2017. Storm overwash  
511      of a gravel barrier: Field measurements and XBeach-G modelling. Coastal  
512      Engineering 120, 22–35.
- 513      Anthony, E.J., Marriner, N., Morhange, C., 2014. Human influence and the  
514      changing geomorphology of Mediterranean deltas and coasts over the last  
515      6000 years: From progradation to destruction phase? Earth-Science Reviews  
516      139, 336–361.
- 517      Bayram, A., Larson, M., Miller, H.C., Kraus, N.C., 2001. Cross-shore distribu-  
518      tion of longshore sediment transport: comparison between predictive formulas  
519      and field measurements. Coastal Engineering 44, 79–99.
- 520      Berek, E.P., Dean, R.G., 1982. Field investigation of longshore transport dis-  
521      tribution, in: Coastal Engineering Proceedings, 1(18).
- 522      Bergillos, R.J., López-Ruiz, A., Ortega-Sánchez, M., Masselink, G., Losada,  
523      M.A., 2016a. Implications of delta retreat on wave propagation and longshore

- 524 sediment transport - Guadalfeo case study (southern Spain). *Marine Geology*  
525 382, 1–16.
- 526 Bergillos, R.J., Masselink, G., McCall, R.T., Ortega-Sánchez, M., 2016b. Mod-  
527 ellng overwash vulnerability along mixed sand-gravel coasts with XBeach-G:  
528 Case study of Playa Granada, southern Spain, in: *Coastal Engineering Pro-*  
529 *ceedings*.
- 530 Bergillos, R.J., Ortega-Sánchez, M., 2017. Assessing and mitigating the land-  
531 scape effects of river damming on the Guadalfeo River delta, southern Spain.  
532 *Landscape and Urban Planning* 165, 117–129.
- 533 Bergillos, R.J., Ortega-Sánchez, M., Losada, M.A., 2015a. Foreshore evolution  
534 of a mixed sand and gravel beach: The case of Playa Granada (Southern  
535 Spain), in: *Proceedings of the 8th Coastal Sediments*, World Scientific.
- 536 Bergillos, R.J., Ortega-Sánchez, M., Masselink, G., Losada, M.A., 2015b. Ur-  
537 ban planning analysis of Mediterranean deltas - Guadalfeo case study, in:  
538 12th International Conference on the Mediterranean Coastal Environment,  
539 pp. 143–154.
- 540 Bergillos, R.J., Ortega-Sánchez, M., Masselink, G., Losada, M.A., 2016c.  
541 Morpho-sedimentary dynamics of a micro-tidal mixed sand and gravel beach,  
542 Playa Granada, southern Spain. *Marine Geology* 379, 28–38.
- 543 Bergillos, R.J., Rodríguez-Delgado, C., López-Ruiz, A., Millares, A., Ortega-  
544 Sánchez, M., Losada, M.A., 2015c. Recent human-induced coastal changes  
545 in the Guadalfeo river deltaic system (southern Spain), in: *Proceedings of*  
546 *the 36th IAHR-International Association for Hydro-Environment Engineering*  
547 *and Research World Congress*: <http://89.31.100.18/~iahrpapers/87178.pdf>.
- 548 Bergillos, R.J., Rodríguez-Delgado, C., Millares, A., Ortega-Sánchez, M.,

- 549 Losada, M.A., 2016d. Impact of river regulation on a Mediterranean delta: as-  
550 sessment of managed versus unmanaged scenarios. *Water Resources Research*  
551 52, 5132–5148.
- 552 Bergillos, R.J., Rodríguez-Delgado, C., Ortega-Sánchez, M., 2017. Advances  
553 in management tools for modeling artificial nourishments in mixed beaches.  
554 *Journal of Marine Systems*, 172, 1–13.
- 555 Bowden, K.F., 1983. Physical oceanography of coastal waters. Ellis Horwood  
556 Ltd., Chichester England.
- 557 Bramato, S., Ortega-Sánchez, M., Mans, C., Losada, M.A., 2012. Natural re-  
558 covery of a mixed sand and gravel beach after a sequence of a short duration  
559 storm and moderate sea states. *Journal of Coastal Research* 28, 89–101.
- 560 Buscombe, D., Masselink, G., 2006. Concepts in gravel beach dynamics. *Earth-  
561 Science Reviews* 79, 33–52.
- 562 Carter, R.W.G., Orford, J.D., 1984. Coarse clastic barrier beaches: a discussion  
563 of the distinctive dynamic and morphosedimentary characteristics. *Develop-  
564 ments in Sedimentology* 39, 377–389.
- 565 Carter, R.W.G., Orford, J.D., 1991. The sedimentary organisation and be-  
566 haviour of drift-aligned gravel barriers, in: *Proceedings of the 3rd Coastal  
567 Sediments*, ASCE. pp. 934–948.
- 568 Clemmensen, L.B., Glad, A.C., Kroon, A., 2016. Storm flood impacts along  
569 the shores of micro-tidal inland seas: A morphological and sedimentological  
570 study of the Vesterlyng beach, the Belt Sea, Denmark. *Geomorphology* 253,  
571 251–261.
- 572 Clemmensen, L.B., Nielsen, L., 2010. Internal architecture of a raised beach

- 573 ridge system (Anholt, Denmark) resolved by ground-penetrating radar inves-  
574 tigations. *Sedimentary Geology* 223, 281–290.
- 575 Dashtgard, S.E., Gingras, M.K., Butler, K.E., 2006. Sedimentology and stratig-  
576 raphy of a transgressive, muddy gravel beach: Waterside Beach, Bay of Fundy,  
577 Canada. *Sedimentology* 53, 279–296.
- 578 De Alegría-Arzaburu, A.R., Masselink, G., 2010. Storm response and beach  
579 rotation on a gravel beach, Slapton Sands, UK. *Marine Geology* 278, 77–99.
- 580 Dean, R.G., Dalrymple, R.A., 2002. Coastal processes with engineering appli-  
581 cations. Cambridge University Press, New York.
- 582 Deltares, 2014. XBeach-G GUI 1.0. User Manual. Delft, The Netherlands.
- 583 Engels, S., Roberts, M.C., 2005. The architecture of prograding sandy-gravel  
584 beach ridges formed during the last Holocene highstand: Southwestern British  
585 Columbia, Canada. *Journal of Sedimentary Research* 75, 1052–1064.
- 586 Félix, A., Baquerizo, A., Santiago, J.M., Losada, M.A., 2012. Coastal zone  
587 management with stochastic multi-criteria analysis. *Journal of Environmental  
588 Management* 112, 252–266.
- 589 Forbes, D.L., Orford, J.D., Carter, R.W.G., Shaw, J., Jennings, S.C., 1995.  
590 Morphodynamic evolution, self-organisation, and instability of coarse-clastic  
591 barriers on paraglacial coasts. *Marine Geology* 126, 63–85.
- 592 French, J., Burningham, H., 2015. Wave-driven sediment pathways on a gravel-  
593 dominated coast subject to a strongly bi-modal wave climate, Suffolk, eastern  
594 UK, in: *Proceedings of the 8th Coastal Sediments*, World Scientific.
- 595 Holthuijsen, L., Booij, N., Ris, R., 1993. A spectral wave model for the coastal  
596 zone, in: *Ocean Wave Measurement and Analysis*, ASCE. pp. 630–641.

- 597 Horn, D.P., Walton, S.M., 2007. Spatial and temporal variations of sediment  
598 size on a mixed sand and gravel beach. *Sedimentary Geology* 202, 509–528.
- 599 Jamal, M.H., Simmonds, D.J., Magar, V., 2014. Modelling gravel beach dy-  
600 namics with XBeach. *Coastal Engineering* 89, 20–29.
- 601 Jamal, M.H., Simmonds, D.J., Magar, V., Pan, S., 2011. Modelling infiltration  
602 on gravel beaches with an XBeach variant, in: *Coastal Engineering Proceed-*  
603 *ings*, 1(32).
- 604 Jennings, R., Shulmeister, J., 2002. A field based classification scheme for gravel  
605 beaches. *Marine Geology* 186, 211–228.
- 606 Kamphuis, J., 1991. Alongshore sediment transport rate distribution, in: Pro-  
607 ceedings of the 3rd Coastal Sediments, ASCE. pp. 170–183.
- 608 Komar, P.D., 1983. Nearshore currents and sand transport on beaches. Elsevier  
609 oceanography series 35, 67–109.
- 610 Lesser, G.R., 2009. An approach to medium-term coastal morphological mod-  
611 eling. Ph.D. thesis. Department of Civil Engineering, Delft University of  
612 Technology, Delft, The Netherlands.
- 613 Lesser, G.R., Roelvink, J.A., Van Kester, J.A.T.M., Stelling, G.S., 2004. Devel-  
614 opment and validation of a three-dimensional morphological model. *Coastal*  
615 *Engineering* 51, 883–915.
- 616 López de San Román-Blanco, B., 2004. Dynamics of gravel and mixed sand and  
617 gravel beaches. Ph.D. thesis. Imperial College, London, UK.
- 618 López de San Román-Blanco, B., Coates, T.T., Holmes, P., Chadwick, A.J.,  
619 Bradbury, A., Baldock, T.E., Pedrozo-Acuña, A., Lawrence, J., Grüne, J.,  
620 2006. Large scale experiments on gravel and mixed beaches: Experimental

- 621 procedure, data documentation and initial results. Coastal Engineering 53,  
622 349–362.
- 623 López-Ruiz, A., Ortega-Sánchez, M., Baquerizo, A., Losada, M.A., 2014. A  
624 note on alongshore sediment transport on weakly curvilinear coasts and its  
625 implications. Coastal Engineering 88, 143–153.
- 626 Losada, M.A., Baquerizo, A., Ortega-Sánchez, M., Ávila, A., 2011. Coastal  
627 evolution, sea level, and assessment of intrinsic uncertainty. Journal of Coastal  
628 Research , 218–228.
- 629 Mason, T., Voulgaris, G., Simmonds, D.J., Collins, M.B., 1997. Hydrodynamics  
630 and sediment transport on composite (Mixed Sand/Shingle) and sand  
631 beaches: a comparison, in: Proceedings of the 3rd Coastal Dynamics, ASCE.  
632 pp. 48–57.
- 633 Masselink, G., McCall, R.T., Poate, T., Van Geer, P., 2014. Modelling storm  
634 response on gravel beaches using XBeach-G, in: Proceedings of the Institution  
635 of Civil Engineers-Maritime Engineering, Thomas Telford Ltd. pp. 173–191.
- 636 Masselink, G., Russell, P., Blenkinsopp, C., Turner, I.L., 2010. Swash zone  
637 sediment transport, step dynamics and morphological response on a gravel  
638 beach. Marine Geology 274, 50–68.
- 639 Masselink, G., Scott, T., Poate, T., Russell, P., Davidson, M., Conley, D., 2016.  
640 The extreme 2013/2014 winter storms: hydrodynamic forcing and coastal  
641 response along the southwest coast of England. Earth Surface Processes and  
642 Landforms 41, 378–391.
- 643 Matias, A., Blenkinsopp, C.E., Masselink, G., 2014. Detailed investigation of  
644 overwash on a gravel barrier. Marine Geology 350, 27–38.

- 645 McCall, R.T., 2015. Process-based modelling of storm impacts on gravel coasts.  
646 Ph.D. thesis. Plymouth University, UK.
- 647 McCall, R.T., Masselink, G., Poate, T., Bradbury, A., Russell, P., Davidson,  
648 M., 2013. Predicting overwash on gravel barriers. *Journal of Coastal Research*  
649 65, 1473–1478.
- 650 McCall, R.T., Masselink, G., Poate, T.G., Roelvink, J.A., Almeida, L.P., 2015.  
651 Modelling the morphodynamics of gravel beaches during storms with XBeach-  
652 G. *Coastal Engineering* 103, 52–66.
- 653 McCall, R.T., Masselink, G., Poate, T.G., Roelvink, J.A., Almeida, L.P., David-  
654 son, M., Russell, P.E., 2014. Modelling storm hydrodynamics on gravel  
655 beaches with XBeach-G. *Coastal Engineering* 91, 231–250.
- 656 McCall, R.T., Masselink, G., Roelvink, D., Russell, P., Davidson, M., Poate,  
657 T., 2012. Modelling overwash and infiltration on gravel barriers, in: *Coastal*  
658 *Engineering Proceedings*, 1(33).
- 659 Millares, A., Polo, M.J., Moñino, A., Herrero, J., Losada, M.A., 2014. Bedload  
660 dynamics and associated snowmelt influence in mountainous and semiarid  
661 alluvial rivers. *Geomorphology* 206, 330–342.
- 662 Moses, C.A., Williams, R.B.G., 2008. Artificial beach recharge: the South East  
663 England experience. *Zeitschrift für Geomorphologie, Supplementary Issues*  
664 52, 107–124.
- 665 Nielsen, P., Hanslow, D.J., 1991. Wave runup distributions on natural beaches.  
666 *Journal of Coastal Research* 7, 1139–1152.
- 667 Orford, J.D., Anthony, E.J., 2011. Extreme events and the morphodynamics of  
668 gravel-dominated coastal barriers: Strengthening uncertain ground. *Marine*  
669 *Geology* 290, 41–45.

- 670 Orford, J.D., Carter, R.W.G., 1995. Examination of mesoscale forcing of a  
671 swash-aligned, gravel barrier from Nova Scotia. *Marine Geology* 126, 201–  
672 211.
- 673 Orford, J.D., Carter, R.W.G., Jennings, S.C., 1991. Coarse clastic barrier envi-  
674 ronments: evolution and implications for Quaternary sea level interpretation.  
675 *Quaternary International* 9, 87–104.
- 676 Orford, J.D., Carter, R.W.G., McKenna, J., Jennings, S.C., 1995. The rela-  
677 tionship between the rate of mesoscale sea-level rise and the rate of retreat of  
678 swash-aligned gravel-dominated barriers. *Marine Geology* 124, 177–186.
- 679 Orford, J.D., Forbes, D.L., Jennings, S.C., 2002. Organisational controls, ty-  
680 pologies and time scales of paraglacial gravel-dominated coastal systems. *Ge-  
681 omorphology* 48, 51–85.
- 682 Ortega-Sánchez, M., Bergillos, R.J., López-Ruiz, A., Losada, M.A., 2017. Mor-  
683 phodynamics of Mediterranean Mixed Sand and Gravel Coasts. Springer.
- 684 Payo, A., Mukhopadhyay, A., Hazra, S., Ghosh, T., Ghosh, S., Brown, S.,  
685 Nicholls, R.J., Bricheno, L., Wolf, J., Kay, S., Lázár, A.N., Haque, A., 2016.  
686 Projected changes in area of the Sundarban mangrove forest in Bangladesh  
687 due to SLR by 2100. *Climatic Change*, 1–13.
- 688 Pedrozo-Acuña, A., 2005. Concerning swash on steep beaches. Ph.D. thesis.  
689 University of Plymouth, UK.
- 690 Pedrozo-Acuña, A., Simmonds, D.J., Chadwick, A.J., Silva, R., 2007. A  
691 numerical–empirical approach for evaluating morphodynamic processes on  
692 gravel and mixed sand–gravel beaches. *Marine Geology* 241, 1–18.
- 693 Pedrozo-Acuña, A., Simmonds, D.J., Otta, A.K., Chadwick, A.J., 2006. On the  
694 cross-shore profile change of gravel beaches. *Coastal Engineering* 53, 335–347.

- 695 Poate, T., Masselink, G., Davidson, M., McCall, R.T., Russell, P., Turner, I.,  
696 2013. High frequency in-situ field measurements of morphological response  
697 on a fine gravel beach during energetic wave conditions. *Marine Geology* 342,  
698 1–13.
- 699 Poate, T.G., McCall, R.T., Masselink, G., 2016. A new parameterisation for  
700 runup on gravel beaches. *Coastal Engineering* 117, 176–190.
- 701 Pontee, N.I., Pye, K., Blott, S.J., 2004. Morphodynamic behaviour and sedi-  
702 mentary variation of mixed sand and gravel beaches, Suffolk, UK. *Journal of*  
703 *Coastal Research* 20, 256–276.
- 704 Shaw, J., Taylor, R.B., Forbes, D.L., 1990. Coarse clastic barriers in eastern  
705 Canada: patterns of glaciogenic sediment dispersal with rising sea levels.  
706 *Journal of Coastal Research* 9, 160–200.
- 707 Shulmeister, J., Kirk, R.M., 1993. Evolution of a mixed sand and gravel barrier  
708 system in North Canterbury, New Zealand, during Holocene sea-level rise and  
709 still-stand. *Sedimentary Geology* 87, 215–235.
- 710 Soons, J.M., Shulmeister, J., Holt, S., 1997. The Holocene evolution of a well  
711 nourished gravelly barrier and lagoon complex, Kaitorete Spit, Canterbury,  
712 New Zealand. *Marine Geology* 138, 69–90.
- 713 Spencer, T., Schuerch, M., Nicholls, R.J., Hinkel, J., Lincke, D., Vafeidis, A.T.,  
714 Reef, R., McFadden, L., Brown, S., 2016. Global coastal wetland change under  
715 sea-level rise and related stresses: the diva wetland change model. *Global and*  
716 *Planetary Change* 139, 15–30.
- 717 Syvitski, J.P.M., Vörösmarty, C.J., Kettner, A.J., Green, P., 2005. Impact of  
718 humans on the flux of terrestrial sediment to the global coastal ocean. *Science*  
719 308, 376–380.

- 720 Van Rijn, L., Walstra, D., Grasmeijer, B., Sutherland, J., Pan, S., Sierra, J.,  
721 2003. The predictability of cross-shore bed evolution of sandy beaches at the  
722 time scale of storms and seasons using process-based profile models. Coastal  
723 Engineering 47, 295–327.
- 724 Van Rijn, L.C., 2014. A simple general expression for longshore transport of  
725 sand, gravel and shingle. Coastal Engineering 90, 23–39.
- 726 Van Rijn, L.C., Sutherland, J.R., 2011. Erosion of gravel barriers and beaches,  
727 in: Proceedings of the 7th Coastal Sediments, World Scientific.
- 728 Van Wellen, E., Chadwick, A.J., Mason, T., 2000. A review and assessment of  
729 longshore sediment transport equations for coarse-grained beaches. Coastal  
730 Engineering 40, 243–275.
- 731 Van Wellen, E., Shadwick, A.J., Lee, M., Baily, B., Morfett, J., 1998. Evaluation  
732 of longshore sediment transport models on coarse grained beaches using  
733 field data: A preliminary investigation, in: Coastal Engineering Proceedings,  
734 1(26).
- 735 Williams, J.J., de Alegría-Arzaburu, A.R., McCall, R.T., Van Dongeren, A.,  
736 2012. Modelling gravel barrier profile response to combined waves and tides  
737 using XBeach: Laboratory and field results. Coastal Engineering 63, 62–80.

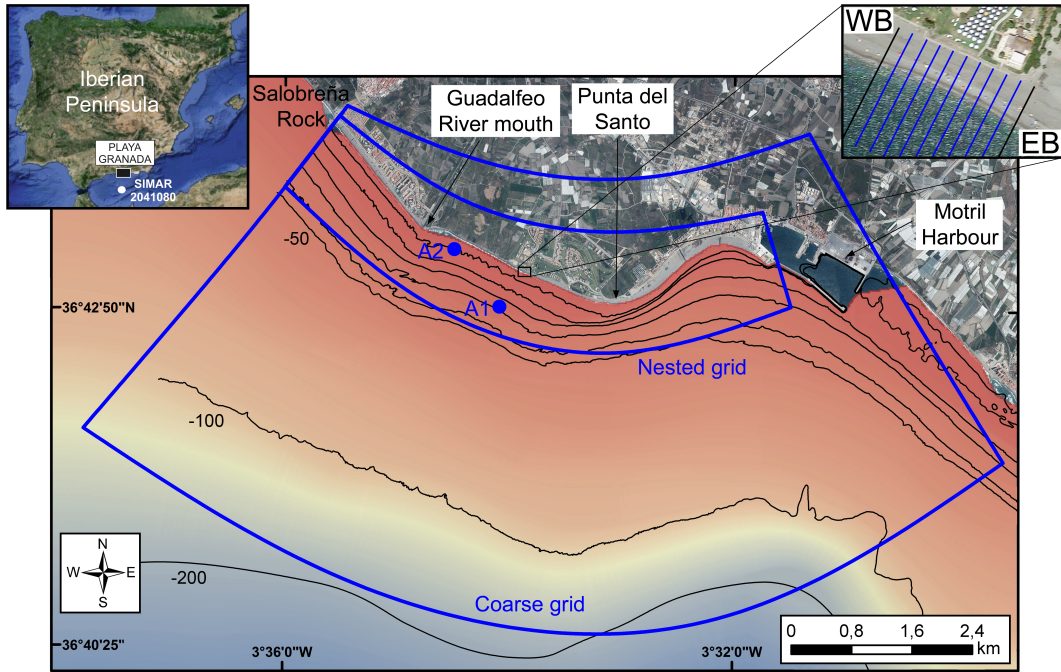


Figure 1: Upper left panel: Location of the study site (Playa Granada, southern Spain) and the SIMAR point 2041080. Central panel: bathymetric contours, grids used in the wave propagation model and positioning of the ADCPs (A1 and A2). Upper right panel: west (WB) and east (EB) boundaries of the surveyed area and measured beach profiles.

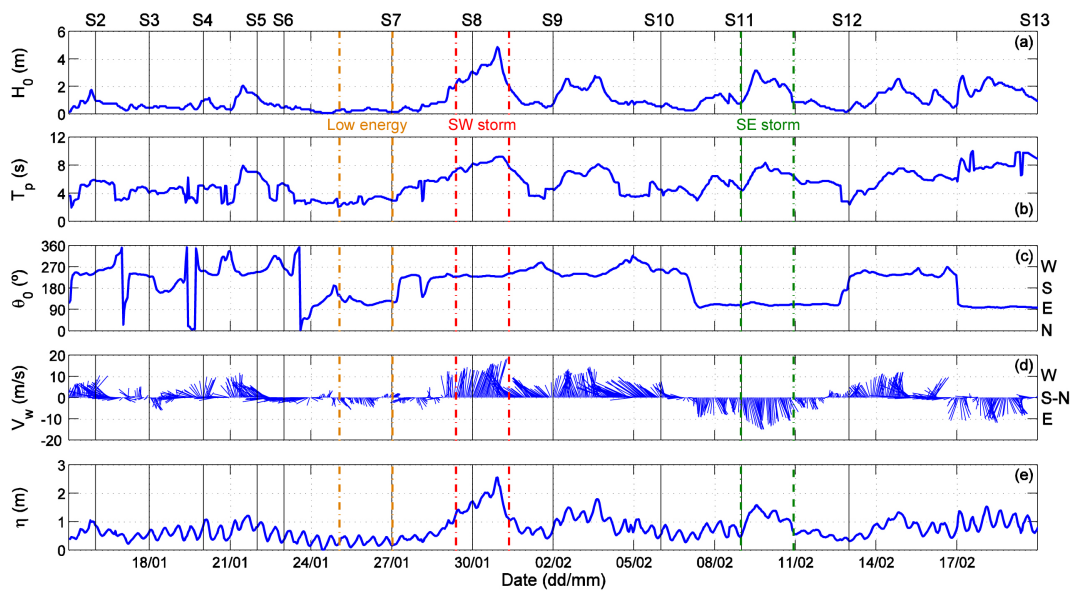


Figure 2: Evolution of the deep-water significant wave height (a), spectral peak period (b), wave direction (c), wind velocity and direction (d), and total run-up (e) over the study period. The vertical black lines indicate the date of the field surveys and the vertical coloured lines delimitate the windows selected to model the profile response.

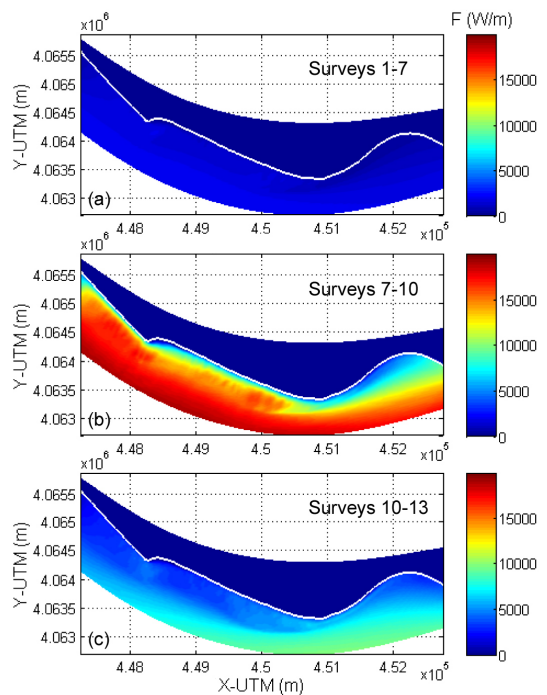


Figure 3: Spatial distribution of the time-averaged energy flux (in W/m) modelled with Delft3D-WAVE: (a) surveys 1-7 (low energy conditions), (b) surveys 7-10 (south-westerly storm), and (c) surveys 10-13 (south-easterly storm). The shorelines are highlighted in white.

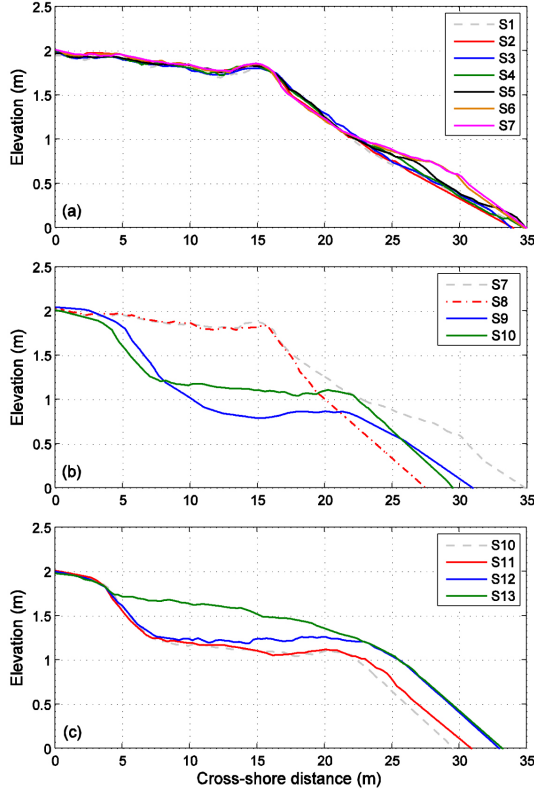


Figure 4: Evolution of the upper profile during the study period: (a) surveys 1-7 (low energy conditions), (b) surveys 7-10 (south-westerly storm), and (c) surveys 10-13 (south-easterly storm). Elevation = 0 indicates the MLWS level.



Figure 5: (a) Beginning of the overwash process during the south-westerly storm (survey 8). (b) Beginning of the south-easterly storm (survey 11).

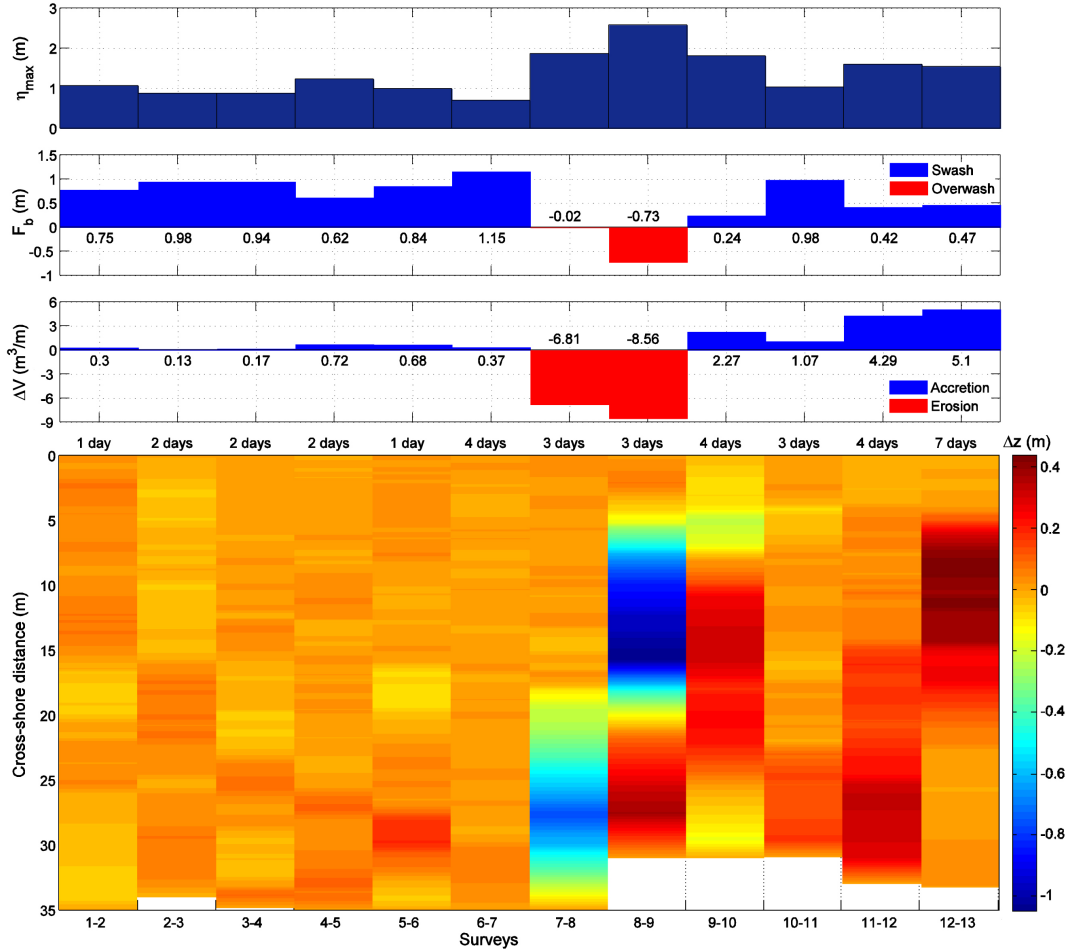


Figure 6: From top to bottom: maximum total run-up before each survey, minimum freeboard before each survey, unit volume differences above the MLWS level between surveys, and bed level changes above the MLWS level between surveys. The number of days between surveys is indicated in the lower panel. The white colour in the lower panel is due to coastline retreat.

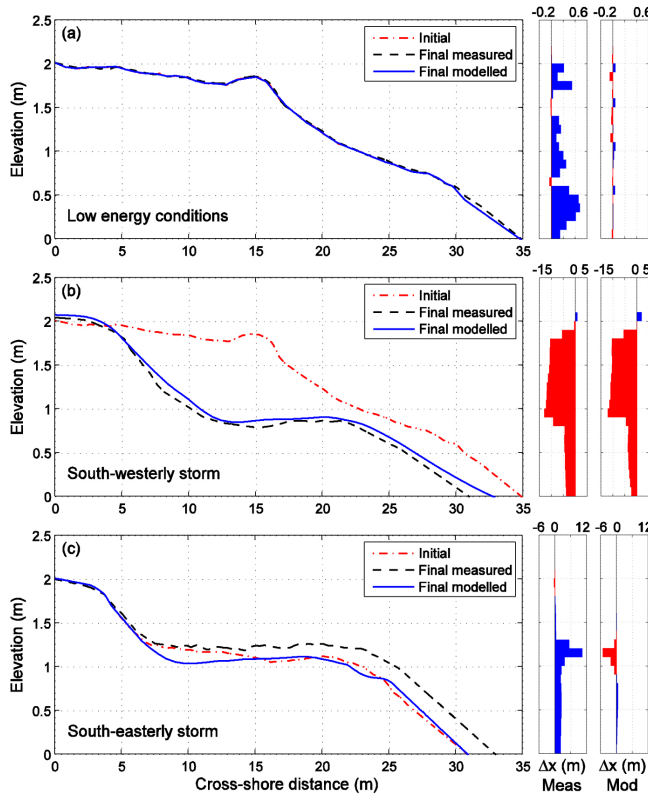


Figure 7: Initial, final measured and final modelled profiles with XBeach-G: (a) low energy conditions window, (b) south-westerly storm, and (c) south-easterly storm. Elevation = 0 indicates the MLWS level. Differences in measured (Meas) and modelled (Mod) cross-shore distances between profiles ( $\Delta x$ ) are indicated in the right panels.

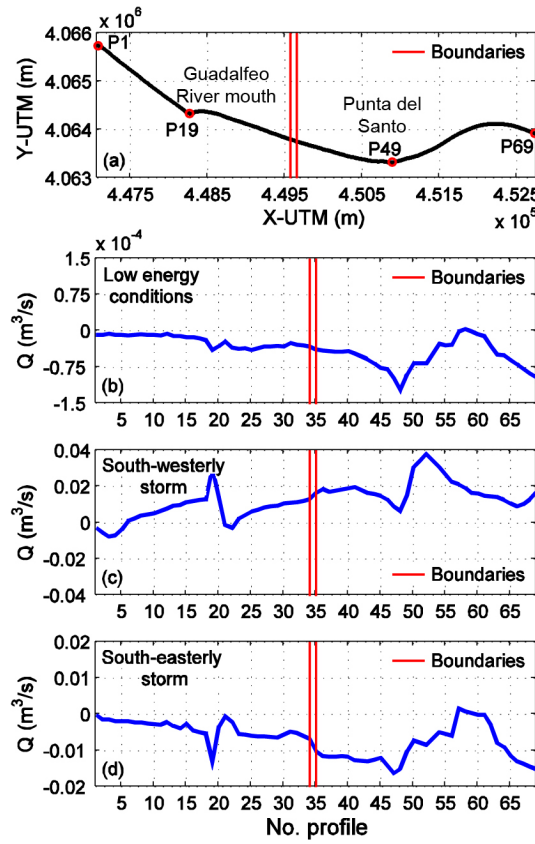


Figure 8: Alongshore evolution of the time-averaged LST rates: (b) low energy conditions window, (c) south-westerly storm, and (d) south-easterly storm. The shoreline and four profile locations are shown in panel a.

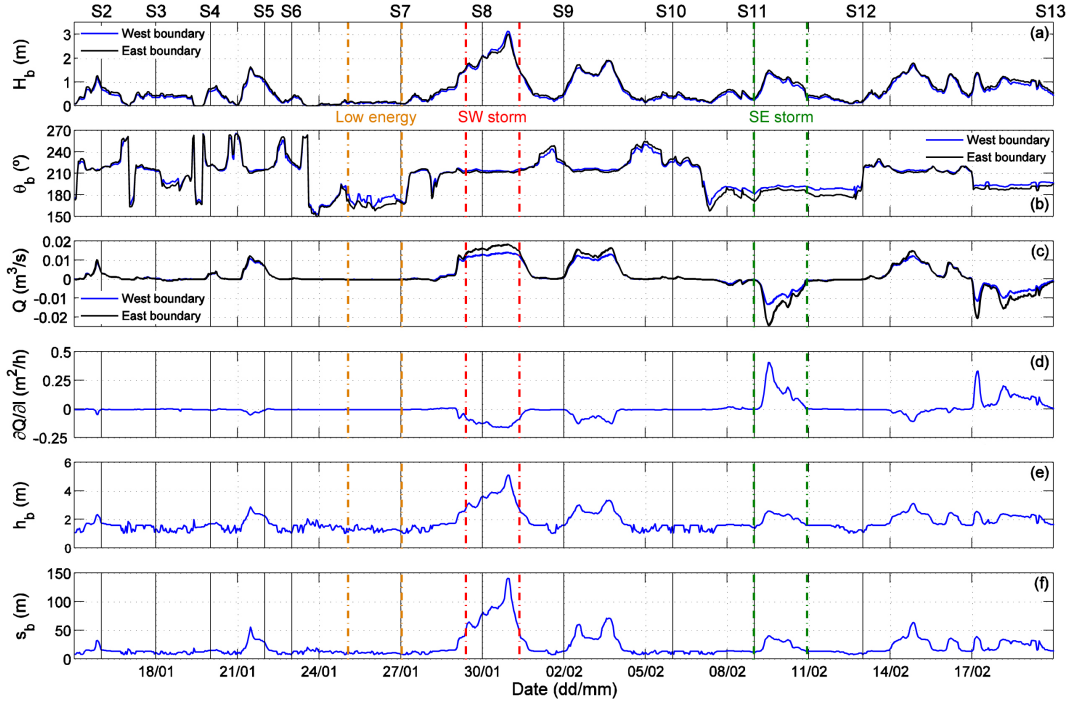


Figure 9: Evolution of the breaking wave height (a), breaking wave direction (b), LST rate (c), LST gradient (d), breaking depth (e), and breaking cross-shore distance (f) during the study period. The vertical black lines indicate the date of the field surveys and the vertical coloured lines delimitate the windows selected to model the profile response.

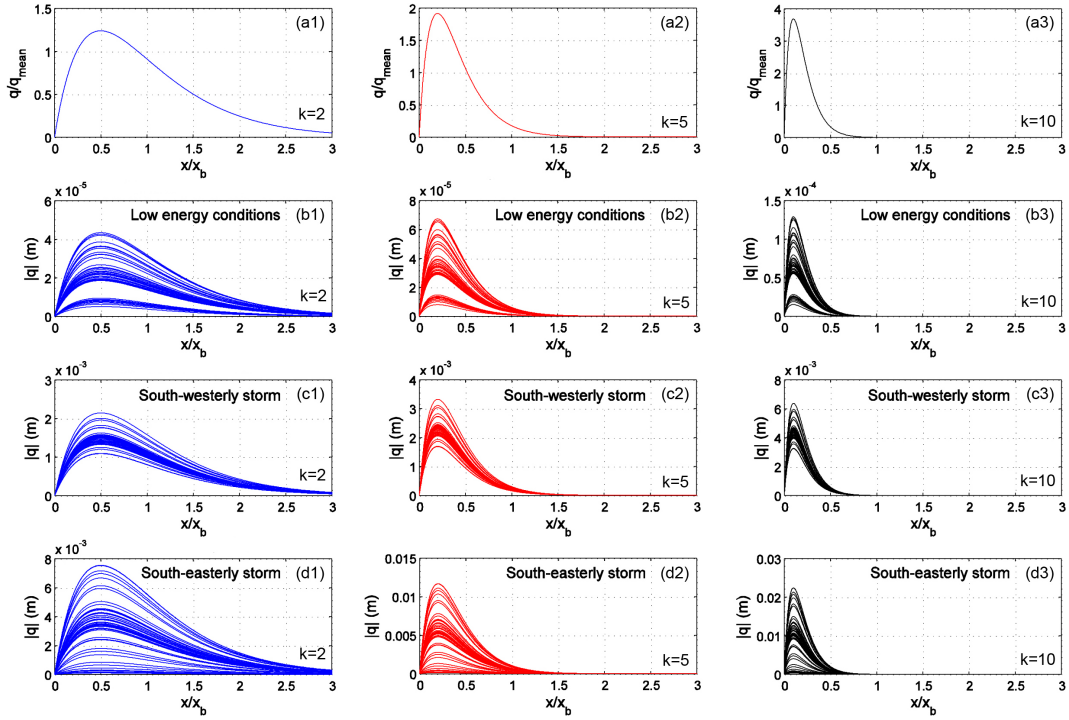


Figure 10: Normalized cross-shore distribution of LST for  $k = 2$  (a1),  $k = 5$  (a2), and  $k = 10$  (a3). Cross-shore distribution during the low energy conditions window (b), the south-westerly storm (c), and the south-easterly storm (d) for  $k=2$  (1),  $k=5$  (2), and  $k=10$  (3).

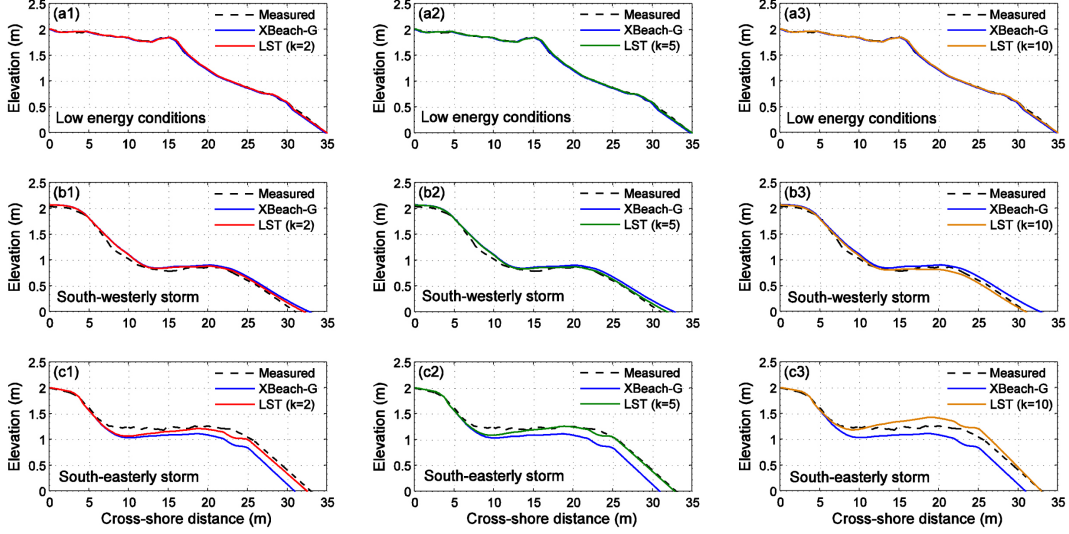


Figure 11: Initial, final measured and final modelled profiles with XBeach-G and LST: (a) low energy conditions window, (b) south-westerly storm, and (c) south-easterly storm for  $k = 2$  (1),  $k = 5$  (2), and  $k = 10$  (3). Elevation = 0 indicates the MLWS level.

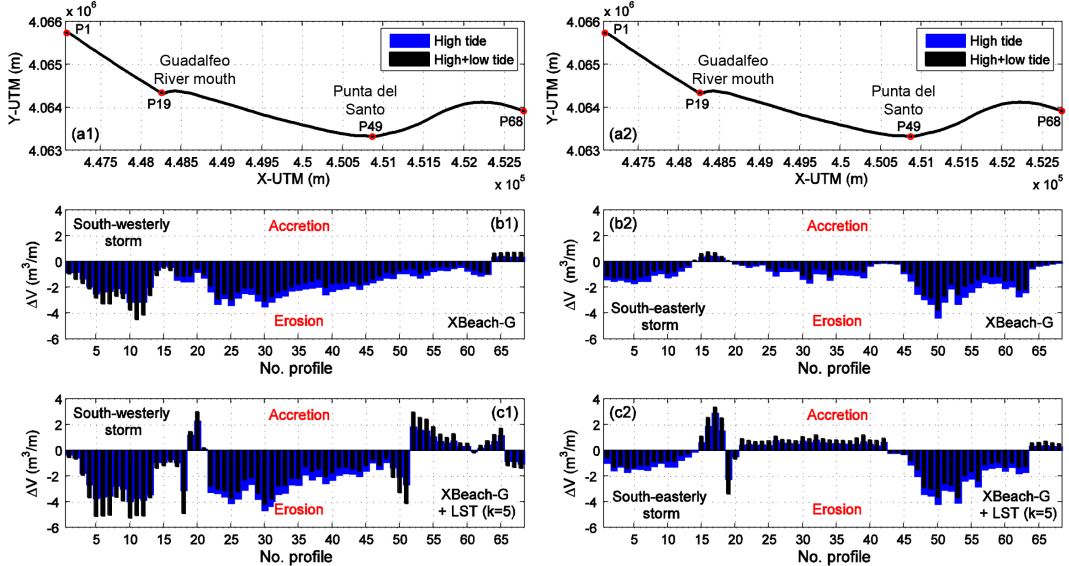


Figure 12: Alongshore evolution of the modelled volumetric changes on the beach (above the MLWS level) with XBeach-G (b) and coupling XBeach and LST (c) for south-westerly (1) and south-easterly (2) storm conditions. The shoreline and four profile locations are shown in panels a1 and a2.